sensors

MDPI

Article

Green Phosphorene as a Promising Biosensor for Detection of Furan and p-Xylene as Biomarkers of Disease: A DFT Study

Aref Aasi [1,*], Erfan Aasi [2], Sadegh Mehdi Aghaei [1] and Balaji Panchapakesan [1]

[1] Small Systems Laboratory, Department of Mechanical Engineering, Worcester Polytechnic Institute, Worcester, MA 01609, USA; sagh0203@fb.com (S.M.A.); bpanchapakesan@wpi.edu (B.P.)
[2] Department of Mechanical Engineering, Boston University, Boston, MA 02215, USA; eaasi@bu.edu
* Correspondence: aaasi@wpi.edu

Abstract: In this work, Green Phosphorene (GP) monolayers are studied as an electronic sensing element for detecting prostate cancer biomarkers from human urine. The adsorption of furan, C_8H_{10} (p-xylene), and H_2O on pristine GP and S- and Si-doped GP are investigated using the density functional theory (DFT) calculation. Furan and C_8H_{10} molecules have been considered as important biomarkers of prostate cancer patients. First-principles DFT calculations are applied, and the results divulged that pristine GP could be a promising candidate for furan and C_8H_{10} detection. It is manifested that furan and C_8H_{10} are physisorbed on the S-, and Si-doped GP with small adsorption energy and negligible charge transfer. However, the calculations disclose that furan and C_8H_{10} are chemically adsorbed on the pristine GP with adsorption energy of −0.73, and −1.46 eV, respectively. Moreover, we observe that a large charge is transferred from furan to the pristine GP with amount of −0.106 e. Additionally, pristine GP shows short recovery time of 1.81 s at room temperature under the visible light, which make it a reusable sensor device. Overall, our findings propose that the pristine GP sensor is a remarkable candidate for sensing of furan and other biomarkers of prostate cancer in the urine of patients.

Keywords: prostate cancer; green phosphorene; sensor; DFT study; cancer biomarker

Citation: Aasi, A.; Aasi, E.; Mehdi Aghaei, S.; Panchapakesan, B. Green Phosphorene as a Promising Biosensor for Detection of Furan and p-Xylene as Biomarkers of Disease: A DFT Study. *Sensors* **2022**, *22*, 3178. https://doi.org/10.3390/s22093178

Academic Editor: Antonio Di Bartolomeo

Received: 28 March 2022
Accepted: 19 April 2022
Published: 21 April 2022

1. Introduction

The analysis of urine enables the observation of biochemical processes and metabolic products in the human body, as a non-invasive method for screening disease states [1–3]. Human urine is composed of different molecules and analytes, and Volatile Organic Compounds (VOCs) are a fraction of the molecules among them. The odor signature of urine is produced by VOC substances, which carry information on physiological and metabolic status [4–6].

Today, over 279 kinds of VOCs (Furan, p-Xylene, aldehydes, ketones, etc.) have been identified in human urine that can be used as "urine-marks" to provide vital information about dysfunction or metabolic disorders in the human body [7,8]. Detection of VOCs in urine is a significant indicator for monitoring health conditions; hence, developing a suitable platform for this purpose is necessary [9–11].

Many studies have reported that canines can be trained to detect breast, lung, and ovarian cancers from breath, and urine samples [12–14]. It has been shown that variations in the concentration of VOCs from the breath and urine are potentially correlated with various types of diseases and cancers [15–17]. In this regard, scientists have demonstrated that urinary VOC patterns in cancer patients are often different from those found in the urine samples of control subjects, and these differences depend on cancer type and stage [18–20]. One of the leading types of cancer among men is prostate cancer, and furan and p-Xylene (C_8H_{10}) are reported biomarkers for this cancer [21,22]. While 5-year survival rates are nearly 100% for localized and regional prostate cancers, they are only 30% for distant

prostate cancer. Sensors that could detect VOCs from breath and urine could indeed reduce the mortality rate for prostate cancers.

Semiconductor sensor technology based on nanomaterials is one of the latest methods in the field of urine analysis and detection of VOCs [21,23–25]. Since the introduction of graphene as the first 2D material, nanomaterial-based sensors have provided new opportunities in different fields, due to their unique properties [26,27]. Recently, Green Phosphorene (GP), as a novel 2D material and new allotrope of black phosphorene, has been theoretically proposed, and it has enticed considerable attention because of its exceptional characteristics of energy stability, tunable direct bandgap, and strong anisotropy. These properties have made it a great candidate in electronic, optical, catalysis, and sensing applications [28,29].

There have been several studies on the sensing capabilities of black phosphorene in the literature, but there are few theoretical studies regarding the molecule sensing application of GP. It offers faster electronic transport at room temperature and higher directional electronic anisotropy in comparison with the black phosphorene [30]. Inspired by these advantages, Mao et al. [31] theoretically investigated the sensitivity of GP toward inorganic compounds, such as NH_3, SO_2, HCN, and O_3 molecules. They showed that GP could be a potential candidate for O_3 detection. Kaewmaraya et al. [32] utilized theoretical DFT-based calculations to study interaction of GP with small molecules. They explored CO, CO_2, NH_3, NO, NO_2, and H_2O as major environmental molecules. In another study, [33], the interaction of GP with ethanol and methanol vapors based on theoretical DFT calculations are investigated. They suggested that GP nanosheet could be used as a platform to detect the existence of methanol and ethanol vapors. Very recently, our group theoretically examined the sensing properties of GP toward dissolved gases in oil transformers such as H_2, CH_4, and C_2H_2 and the findings manifested that GP could be used for the detection of these molecules [34].

Motivated by the fascinating structural and electronic properties of GP, in this paper, the interaction of GP with furan and p-Xylene, along with H_2O as main interfering molecule in the urine are investigated. We utilize GP monolayer for detection of the targeted molecules, based on the first-principles method (DFT). Different structures of GP, such as pristine and doped GP, are systematically researched and we scrutinize the adsorption behaviors of the molecules with the GP-based nanosensor. Our results demonstrate the promising future of GP-based sensors in the development of high-performance room temperature VOC analyzers for detection of prostate cancer.

2. Computational Details

During this work, all DFT calculations were performed employing Atomistix ToolKit (ATK) package, associated with Non-Equilibrium Green's Function (NEGF) [35–37].

The exchange-correlation functional was approximated using the Perdew–Burke–Ernzerhof (PBE) formalism. Additionally, the Van der Waals (VdW) and long-range interactions were considered by adopting Grimme (DFT-D2) algorithm. The adsorption of the molecules upon pristine or doped GP was found by adsorption energy, where the adsorption energy was calculated by:

$$E_{ad} = E_{Doped-GreenP+molecule} - (E_{Doped-GreenP} + E_{molecule}) \quad (1)$$

where $E_{Doped-GreenP+molecule}$, $E_{Doped-GreenP}$, and $E_{molecule}$ represent the energies for the pristine or doped GP-molecule system, pristine or doped GP, and the corresponding single molecule, respectively. The negative adsorption energy means that the process is exothermic, and its most negative value indicates that the adsorption process is energetically favorable. It is generally believed that chemisorption occurs when the absolute value of adsorption energy is greater than 0.8 eV [38,39].

The optimized lattice parameters of the bulk of GP were determined to be 10.62, 3.26, 7.93 Å along x, y, and z directions, respectively, and are in reasonable accordance with previous studies [32,33]. The supercell extended with a vacuum space size of 20 Å along

the z-direction is considered to prevent image–image interactions. All the modeling was implemented on the sufficient supercell GP with dimensions of 13.82 × 13.25 Å^2.

The basis set of Fritz-Haber-Institute (FHI) pseudopotentials with double-ζ polarized was employed for the calculations. In these calculations, 45 Hartree was set for the kinetic energy mesh cut-off. The convergence criteria of maximum force and maximum stress were set to 0.01 eV/Å and 0.001 eV/Å^3, respectively. For sampling of the Brillouin zone, Monkhorst–Pack k-point was set as 20 × 20 × 1. The electronic properties of the configurations are investigated by the analysis of DOS and a 21 × 21 × 1 k-point was used.

Moreover, using Hartwigsen–Goedecker–Hutter (HGH) pseudopotentials with Tier 3 basis set, the charge transfer (Q) after adsorption of the molecule on the pristine or doped-GP sheet was calculated by employing Mulliken population analysis, where a negative Q demonstrates a charge conveyed from the molecule to the GP sheet, whereas a positive Q shows that the molecule extracts electrons from the sheet.

3. Results and Discussions

First, the optimized geometries of the molecules and the GP monolayer were obtained, and the results are depicted in Figure 1. It can be observed that the monolayer GP is a semiconductor and has an energy band gap of 1.06 eV [40–42]. Additionally, the optimized geometry of the considered molecules furan, C_8H_{10} (p-Xylene), and H_2O are shown in Figure 1. The full relaxation of the geometry of isolated furan gives C:C~1.37 Å, C:H~1.10 Å, and C:O~1.36 Å, which is in accordance with the experimental data [43]. Moreover, the optimized geometry of isolated C_8H_{10} gives C:C~1.40 Å (on the benzene ring), C:H~1.10 Å, and C:C~1.51 Å (on the two sides), which is in good agreement with previous studies [44].

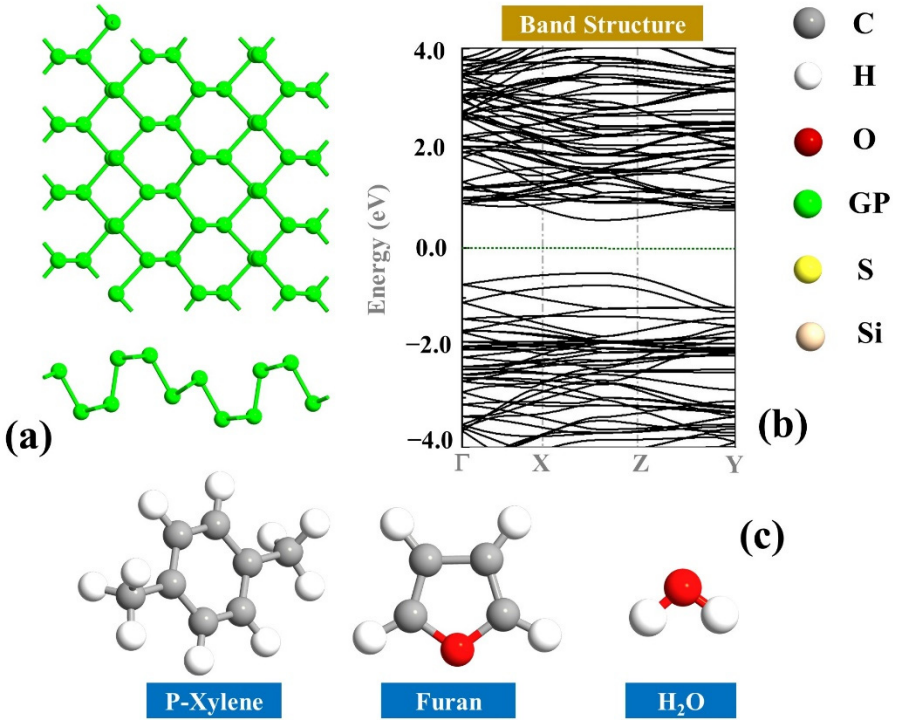

Figure 1. Illustration of (**a**) monolayer GP (top and side views), (**b**) band structure of the GP, and (**c**) structures of p-Xylene (C_8H_{10}), furan, and H_2O molecules.

It is well known that nanomaterials such as GP prepared by the available fabrication methods are likely to have many defects. Additionally, they could be deliberately or accidentally doped with elements like S, and Si. Next, the interactions of S, and Si dopant upon GP were investigated. Two dopants (S, and Si) were introduced to the host material's (GP) surface [32], and different potential points were examined; the most energetically optimized configurations are demonstrated in Figure 2.

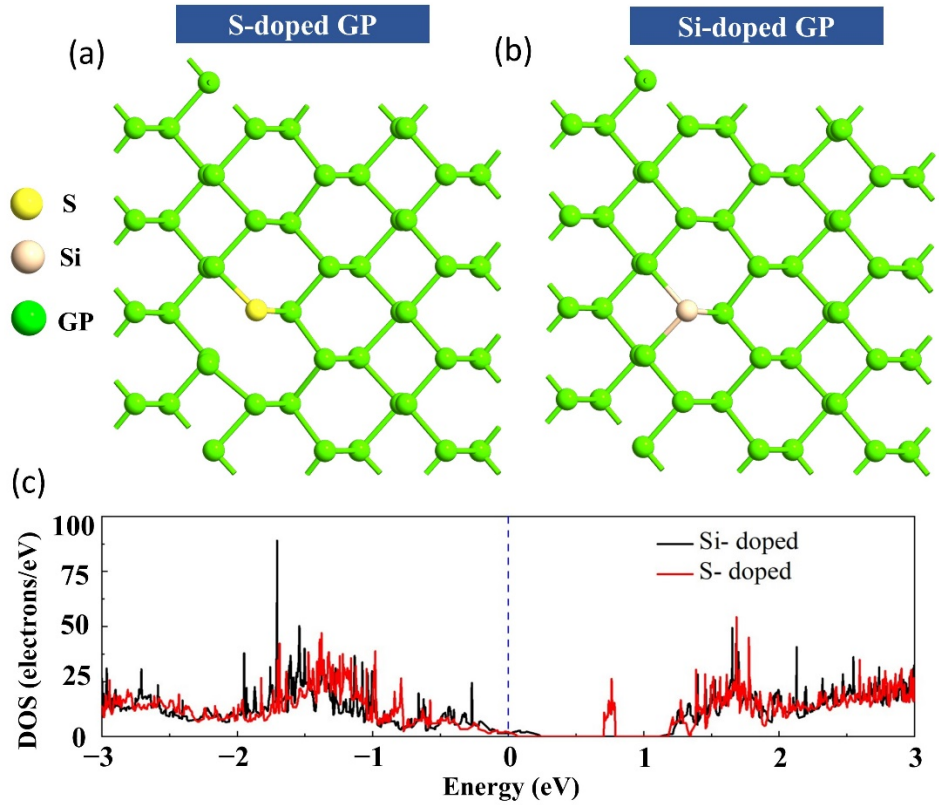

Figure 2. The relaxed atomic structures of (**a**) S-doped and (**b**) Si-doped GP sheet, along with (**c**) DOS calculations.

Interestingly, it can be seen from Figure 2 that after doping the GP with the S atom, the structure underwent a distortion due to the comparable atomic sizes of the dopants with the phosphorus atom, while the bond of S with one of the adjacent P atoms was deteriorated.

Doping considerably impacts DOS, particularly the states close to the Fermi level. The DOS values for two dopant cases are shown in Figure 2. These changes are justified by the fact that GP possesses the sp^3 hybrid character, and each P atom consists of a non-bonding lone pair of electrons that may engage with the frontier p-states of the dopants, and the S and Si doping cause the GP to convert to n-, and p-type semiconductors, respectively.

With the aim of obtaining the preferential adsorption sites of the molecules on the pristine GP, the molecules were placed at a distance of 2 Å above different locations of the sheet with diverse molecular orientations. Various adsorption sites on the GP surface, such as above the P hexagon, the P-P bond, and above the P atom, were studied.

The interaction strength between the sensing material and analytes was evaluated by calculating the adsorption energies, and the most optimized structures are presented in Figure 3. Upon exposure of furan, it adopts a vertical direction, where its O atom is on top of the P atom with a minimum distance of 3.07 Å and an adsorption energy of −0.73 eV (Figure 4). From the electronic band structure calculations (Figure 3), it can be observed that the energy bandgap of the GP (1.06 eV) upon furan adsorption changes to 1 eV.

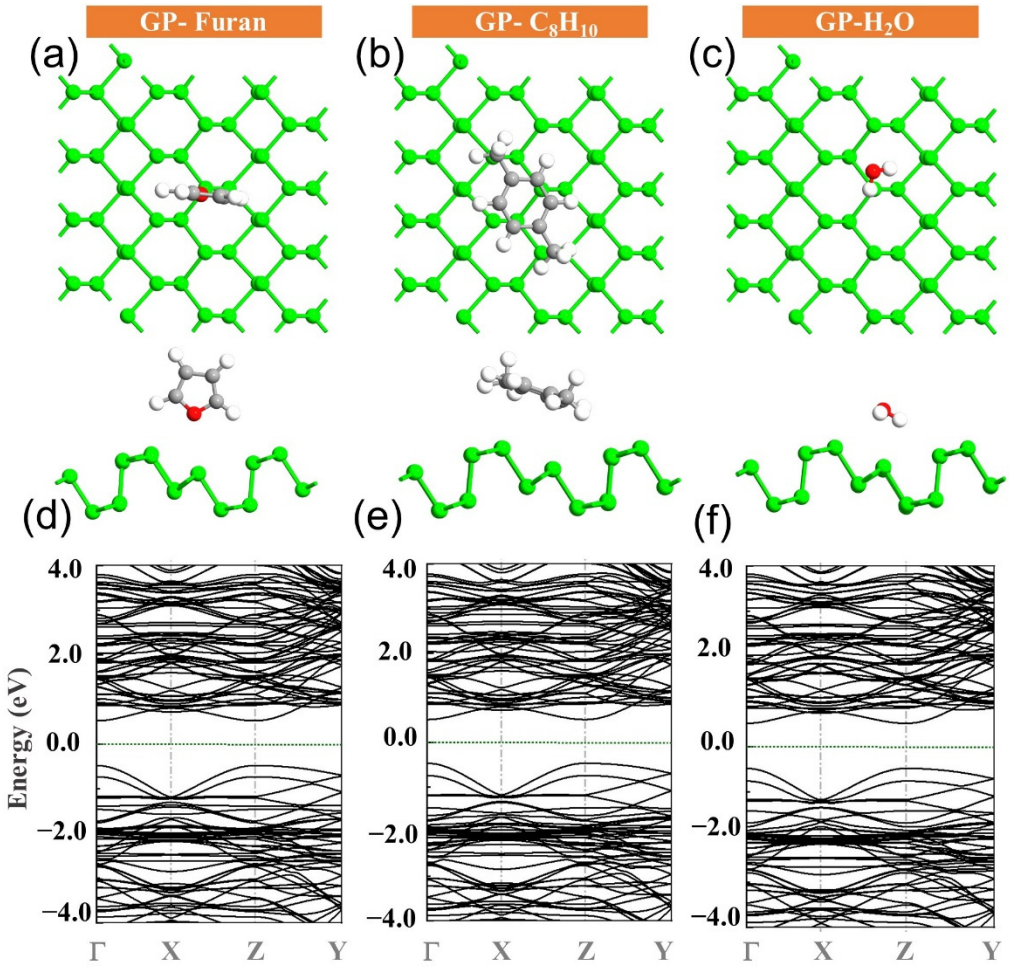

Figure 3. The most stable structures of (**a**) GP-furan, (**b**) GP-C_8H_{10}, and (**c**) GP-H_2O with their corresponding band structures (**d**–**f**).

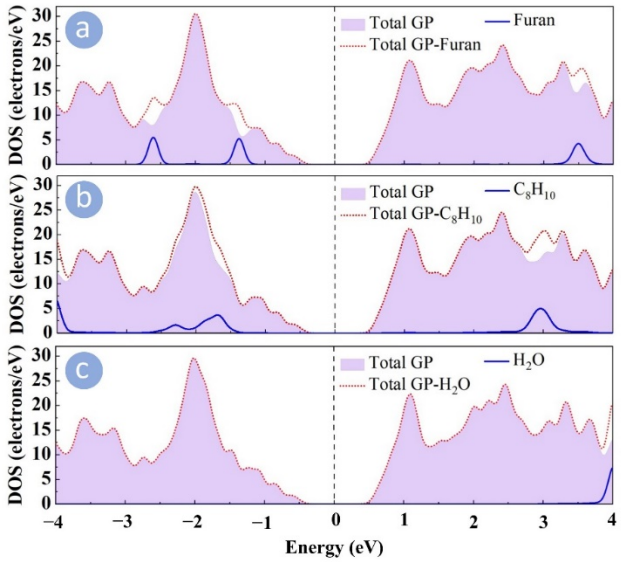

Figure 4. DOS plots for pristine GP sheet exposed to (**a**) furan, (**b**) C_8H_{10}, and (**c**) H_2O molecules.

Moreover, after interaction of the GP with C_8H_{10}, it was adsorbed in a tilted parallel orientation with respect to the plane, with a minimum distance (H-P) of 3.09 Å. Energy of −1.46 eV is emitted after adsorption, and the energy bandgap changes to 0.978 eV. Finally,

H_2O is preferentially adsorbed in this manner, tilted from the horizontal orientation with respect to the GP surface and with the minimum distance of (H-P) 2.92 Å.

The adsorption energy value for H_2O upon interaction with GP, as shown in Table 1, was found to be −0.5 eV. From the electronic band structure, it was determined that the energy bandgap changed to 0.997, and 1 eV, respectively. In addition, all the molecules provided electrons to the surface, so that a total net charge of 0.106 e was achieved for furan. Additionally, GP accepted a total net charge of 0.073 and 0.055 e from C_8H_{10} and H_2O molecules, respectively.

Table 1. The calculated adsorption energy (E_{ad}), interaction distance (D)—i.e., the distance between the molecule and the GP sheet, charge transfer (Q), where negative values of charge indicate a charge transfer from the molecule to the surface, and recovery time (τ).

System	E_{ad} (eV)	D (Å)	Q (*e*)	τ sec @ T = 300 K (Visible Light)	τ sec @ T = 300 K (UV Light)
Pristine GP	-	-	-	-	-
Pristine GP-Furan	−0.73	3.07	−0.106	1.81	1.81×10^{-4}
Pristine GP-C_8H_{10}	−1.46	3.09	−0.073	3.3×10^{12}	3.3×10^{8}
Pristine GP-H_2O	−0.5	2.92	−0.055	2.45×10^{-4}	2.45×10^{-8}
S-doped-GP	-	-	-	-	-
S-doped-GP-Furan	−0.07	2.59	0.027	1.49×10^{-11}	1.49×10^{-15}
S-doped-GP-C_8H_{10}	−1.05	3.50	−0.083	4.3×10^{5}	43.02
S-doped-GP-H_2O	−0.31	2.53	0.003	1.6×10^{-7}	1.6×10^{-11}
Si-doped-GP	-	-	-	-	-
Si-doped-GP-Furan	−0.31	2.82	0.007	1.6×10^{-7}	1.6×10^{-11}
Si-doped-GP-C_8H_{10}	−0.33	3.04	−0.03	3.48×10^{-7}	3.48×10^{-11}
Si-doped-GP-H_2O	−0.16	2.42	0.03	4.86×10^{-10}	4.86×10^{-14}

All of this information, such as net charge transfer and interaction distances for different systems, is detailed in Table 1. To gain a better understanding of molecule adsorption on the GP, the density of states (DOS) of the GP sheet was plotted along with different molecules in Figure 4.

It can be seen that the DOS of the H_2O molecule disappears at around the Fermi level, which indicates that the molecule does not alter the electronic properties of GP, supporting the weak interaction between them. However, in the case of furan and C_8H_{10}, there are overlap peaks between the molecules and the GP, and the nearest peaks to the vicinity of the Fermi level are within the energy spans of −1.5 to −1 eV and −2 to −1.5 eV for furan and C_8H_{10} adsorption, respectively.

To track the adsorption mechanism and to shed light on the adsorption of the molecules upon the GP, recovery time (τ), as a critical factor for the evaluation of the sensor, has to be studied [25,45]. The recovery time τ captures the time cost for the desorption of a target molecule from the sensing material's surface. The τ could be obtained according to the transition state theory and Van't Hoff–Arrhenius explanation:

$$\tau = A^{-1} \exp\left(\frac{-E_{ad}}{BT}\right) \quad (2)$$

where A represents the apparent frequency factor, T is the working temperature, and B is constant of Boltzmann (8.318×10^{-3} kJ/(mol·K)). The ambient temperature (300 K) is considered to gain a full understanding of the desorption properties of the sensor system. The frequency factor was determined to be 10^{12} and 10^{16} Hz, under visible and UV light conditions, respectively [46,47]. Parameter τ for different conditions is tabulated in Table 1.

From Equation (2), it can be observed that sensor devices with a lower value of τ were associated with lower E_{ads} at a given temperature. Thus, the recovery time τ at room temperature (300 K) and under visible light was determined to be 1.81, 3.3×10^{12}, and 2.45×10^{-4} s for furan, C_8H_{10}, and water, respectively. It is important to highlight that both values of τ that are too long and too short are unfavorable for detection in real experiments [47]. As a result, GP is considered to be an option for the detection of furan molecules.

Subsequently, the optimized preferential adsorption configurations for the molecules on the S-, and Si-doped GP were investigated, and the results displayed in Figure 5. After adsorption of furan with S- and Si-doped GP, it was observed that furan adopts a vertical orientation with its H atom pointed toward the surface. There was a minimum distance of 2.59, and 2.82 Å between the H atom of furan and the S and Si atoms, respectively.

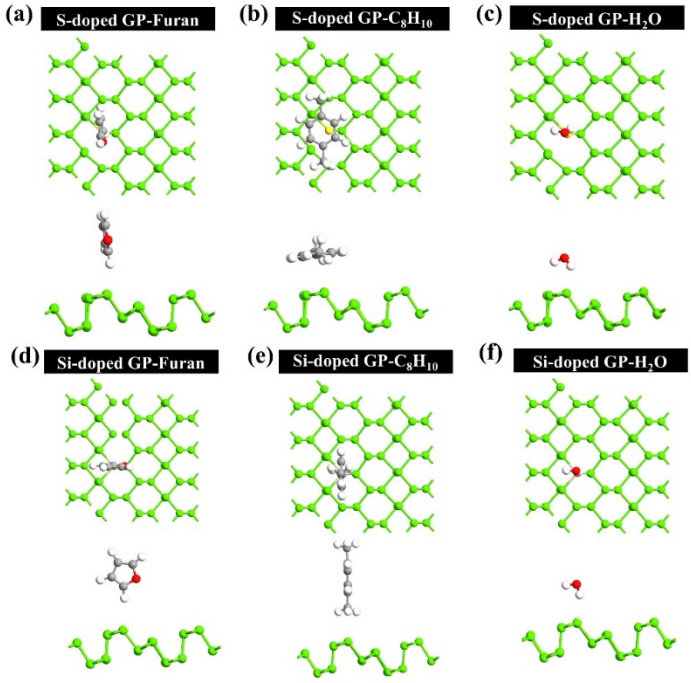

Figure 5. The most relaxed structures for adsorption of molecules on the S-doped and Si-doped GP surface. Configurations of S-doped (**a**) furan (**b**) C_8H_{10} (**c**) H_2O, and Si-doped (**d**) furan (**e**) C_8H_{10} (**f**) H_2O.

Furthermore, in the case of H_2O on both S-, and Si-doped GP, it is adsorbed approximately vertically with respect to the surface of the monolayer, in which there is a minimum distance of 2.53, and 2.42 Å between the H atom and S, and Si atoms, respectively. Nonetheless, C_8H_{10} displays a more complicated adsorption mechanism than other molecules, in such a way that it tends to be adsorbed on the S-doped GP horizontally, with a minimum distance of (H-S) 3.5 Å, and upon Si-doped GP, it is preferentially adsorbed vertically, where its H atoms face down to the Si atom and the surface with a minimum distance of 3.04 Å.

By comprehensively comparing the values of adsorption energy for the configurations, final adsorption energies of −0.07, −1.05, and −0.31 eV were obtained for the adsorption of furan, C_8H_{10}, and H_2O on the S-doped GP, respectively. Additionally, E_{ad} values of −0.31, −0.33, and −0.16 eV were obtained for furan, C_8H_{10}, and H_2O upon Si-doped GP, respectively.

DOS analysis was performed on the doped GP molecules structures, as shown in Figure 6, to further help reveal the nature of the interaction between the molecules and the structures. It can be seen that after adsorption of the molecules upon S- and Si-doped GP, there were no changes around the Fermi level, which suggests that the molecules did not alter the electronic properties of the substrate, supporting the weak interaction between them and the S- and Si-doped sheet.

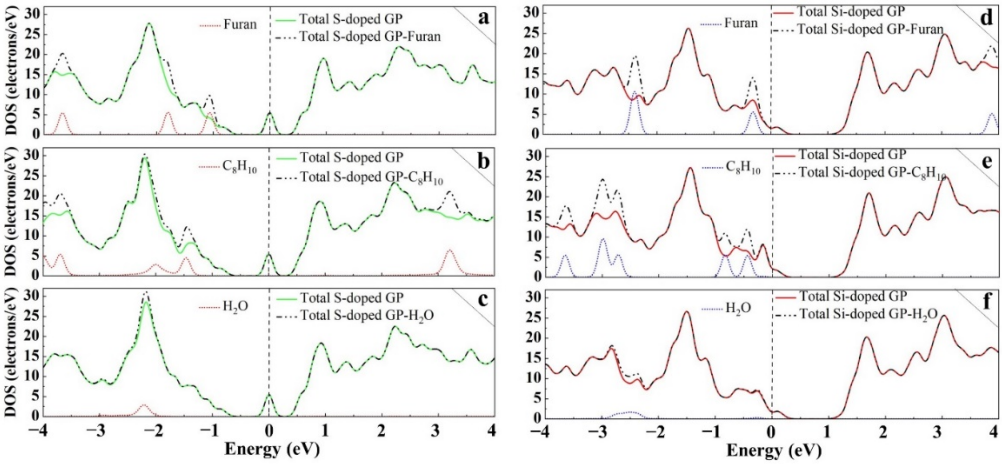

Figure 6. Total DOS curves for S- and Si-doped GP interaction with the molecules. Configurations of S-doped (**a**) furan (**b**) C_8H_{10} (**c**) H_2O, and Si-doped (**d**) furan (**e**) C_8H_{10} (**f**) H_2O.

Considering results obtained for the S- and Si-doped GP, all the molecules were weakly adsorbed onto the doped GP systems. When calculating the recovery time for the corresponding configurations, it can be observed that τ is either too short or too long for desorption of the molecules.

Eventually, the obtained results suggest that pristine GP is a promising factor in molecule sensing. Conversely, the findings show that by introducing atoms (S, and Si) to the GP, its sensitivity toward the prostate biomarkers is not improved, and there is low adsorption energy and negligible charge transfer between the doped GP and the molecules. However, pristine GP appears to be a good candidate for capturing furan and C_8H_{10}, with a moderate adsorption energy of -0.73, and -1.46 eV, large charge transfer, and a quick recovery time.

4. Conclusions

In brief, we employed first-principles computations to analyze the adsorption geometry, adsorption energy, charge transfer, and electronic band structure of GP with the adsorption of several molecules (furan, C_8H_{10}, and H_2O). The results showed that pristine GP could be deployed as a base substrate for adsorbing prostate cancer biomarkers, such as furan and C_8H_{10}. While furan and C_8H_{10} molecules were weakly adsorbed onto the surface of S-, and Si-doped GP, the results indicated that the adsorption energy was low and the charge transfer trivial. The adsorption energy for furan and C_8H_{10} detection by pristine GP was determined to be -0.73 and -1.46 eV, respectively. Additionally, there was high transfer of charges, in an amount of 0.106 and 0.073 e, donated by furan and C_8H_{10} to the GP's surface. Furthermore, it was found that at room temperature and under visible light, pristine GP had a quick recovery time of 1.81 s, making it a reusable sensor for the detection of biomarkers. It is worth mentioning that biological probes are typically water solutions, and the content of water is superior. Therefore, chemical potential of molecules all competing for adsorption sites is concentration dependent. All in all, this study supports GP as a prominent adsorbing substrate for the diagnosis of prostate cancer biomarkers from exhaled breath, and deserves further attention.

Author Contributions: Conceptualization, A.A. and E.A.; methodology, A.A.; software, S.M.A.; validation, A.A., S.M.A. and E.A.; formal analysis, A.A.; investigation, A.A. and E.A.; resources, A.A.; data curation, A.A. and S.M.A.; writing—original draft preparation, A.A. and B.P; writing—review and editing, A.A. and S.M.A.; visualization, A.A.; supervision, B.P.; project administration, B.P.; funding acquisition, B.P. All authors have read and agreed to the published version of the manuscript.

Funding: This research received no external funding.

Institutional Review Board Statement: Not applicable.

Informed Consent Statement: Not applicable.

Data Availability Statement: The data presented in this study are available on request from the corresponding author.

Acknowledgments: B.P. is partially supported by the Fulbright-Nehru scholar program grant number 2021/APE–R/63.

Conflicts of Interest: The authors declare no conflict of interest.

References

1. Khalid, T.; Aggio, R.; White, P.; De Lacy Costello, B.; Persad, R.; Al-Kateb, H.; Jones, P.; Probert, C.S.; Ratcliffe, N. Urinary volatile organic compounds for the detection of prostate cancer. *PLoS ONE* **2015**, *10*, e0143283. [CrossRef] [PubMed]
2. Lima, A.R.; Pinto, J.; Azevedo, A.I.; Barros-Silva, D.; Jerónimo, C.; Henrique, R.; de Lourdes Bastos, M.; de Pinho, P.G.; Carvalho, M. Identification of a biomarker panel for improvement of prostate cancer diagnosis by volatile metabolic profiling of urine. *Br. J. Cancer* **2019**, *121*, 857–868. [CrossRef] [PubMed]
3. Wen, Q.; Boshier, P.; Myridakis, A.; Belluomo, I.; Hanna, G.B. Urinary volatile organic compound analysis for the diagnosis of cancer: A systematic literature review and quality assessment. *Metabolites* **2021**, *11*, 17. [CrossRef] [PubMed]
4. Gao, Q.; Lee, W.-Y. Urinary metabolites for urological cancer detection: A review on the application of volatile organic compounds for cancers. *Am. J. Clin. Exp. Urol.* **2019**, *7*, 232–248.
5. Sethi, S.; Nanda, R.; Chakraborty, T. Clinical application of volatile organic compound analysis for detecting infectious diseases. *Clin. Microbiol. Rev.* **2013**, *26*, 462–475. [CrossRef]
6. Banday, K.M.; Pasikanti, K.K.; Chan, E.C.Y.; Singla, R.; Rao, K.V.S.; Chauhan, V.S.; Nanda, R.K. Use of urine volatile organic compounds to discriminate tuberculosis patients from healthy subjects. *Anal. Chem.* **2011**, *83*, 5526–5534. [CrossRef]
7. Smith, S.; Burden, H.; Persad, R.; Whittington, K.; de Lacy Costello, B.; Ratcliffe, N.M.; Probert, C. A comparative study of the analysis of human urine headspace using gas chromatography—Mass spectrometry. *J. Breath Res.* **2008**, *2*, 037022. [CrossRef]
8. de Lacy Costello, B.; Amann, A.; Al-Kateb, H.; Flynn, C.; Filipiak, W.; Khalid, T.; Osborne, D.; Ratcliffe, N.M. A review of the volatiles from the healthy human body. *J. Breath Res.* **2014**, *8*, 014001. [CrossRef]
9. Aasi, A.; Aghaei, S.M.; Panchapakesan, B. Pt-decorated Phosphorene as a Propitious Room Temperature VOCs Gas Sensor for Sensitive and Selective Detection of Alcohols. *J. Mater. Chem. C* **2021**, *9*, 9242–9250. [CrossRef]
10. Hussain, T.; Sajjad, M.; Singh, D.; Bae, H.; Lee, H.; Larsson, J.A.; Ahuja, R.; Karton, A. Sensing of volatile organic compounds on two-dimensional nitrogenated holey graphene, graphdiyne, and their heterostructure. *Carbon* **2020**, *163*, 213–223. [CrossRef]
11. Aasi, A.; Aghaei, S.M.; Bajgani, S.E.; Panchapakesan, B. Computational Study on Sensing Properties of Pd-Decorated Phosphorene for Detecting Acetone, Ethanol, Methanol, and Toluene—A Density Functional Theory Investigation. *Adv. Theory Simul.* **2021**, *4*, 2100256. [CrossRef]
12. Pickel, D.; Manucy, G.P.; Walker, D.B.; Hall, S.B.; Walker, J.C. Evidence for canine olfactory detection of melanoma. *Appl. Anim. Behav. Sci.* **2004**, *89*, 107–116. [CrossRef]
13. McCulloch, M.; Jezierski, T.; Broffman, M.; Hubbard, A.; Turner, K.; Janecki, T. Diagnostic accuracy of canine scent detection in early-and late-stage lung and breast cancers. *Integr. Cancer Ther.* **2006**, *5*, 30–39. [CrossRef] [PubMed]
14. Horvath, G.; Järverud, G.A.K.; Järverud, S.; Horváth, I. Human ovarian carcinomas detected by specific odor. *Integr. Cancer Ther.* **2008**, *7*, 76–80. [CrossRef] [PubMed]
15. Miekisch, W.; Schubert, J.K.; Noeldge-Schomburg, G.F. Diagnostic potential of breath analysis—Focus on volatile organic compounds. *Clin. Chim. Acta* **2004**, *347*, 25–39. [CrossRef]
16. Mazzone, P.J. Analysis of volatile organic compounds in the exhaled breath for the diagnosis of lung cancer. *J. Thorac. Oncol.* **2008**, *3*, 774–780. [CrossRef]
17. Ruzsányi, V.; Kalapos, M.P. Breath acetone as a potential marker in clinical practice. *J. Breath Res.* **2017**, *11*, 024002. [CrossRef]
18. Shirasu, M.; Touhara, K. The scent of disease: Volatile organic compounds of the human body related to disease and disorder. *J. Biochem.* **2011**, *150*, 257–266. [CrossRef]
19. da Costa, B.R.B.; De Martinis, B.S. Analysis of urinary VOCs using mass spectrometric methods to diagnose cancer: A review. *Clin. Mass Spectrom.* **2020**, *18*, 27–37. [CrossRef]
20. Wagenstaller, M.; Buettner, A. Characterization of odorants in human urine using a combined chemo-analytical and human-sensory approach: A potential diagnostic strategy. *Metabolomics* **2013**, *9*, 9–20. [CrossRef]
21. Sun, X.; Shao, K.; Wang, T. Detection of volatile organic compounds (VOCs) from exhaled breath as noninvasive methods for cancer diagnosis. *Anal. Bioanal. Chem.* **2016**, *408*, 2759–2780. [CrossRef] [PubMed]
22. Jiménez-Pacheco, A.; Salinero-Bachiller, M.; Iribar, M.C.; López-Luque, A.; Miján-Ortiz, J.L.; Peinado, J.M. Furan and p-xylene as candidate biomarkers for prostate cancer. In *Urologic Oncology: Seminars and Original Investigations*; Elsevier: Amsterdam, The Netherlands, 2018; pp. e221–e243.
23. Konvalina, G.; Haick, H. Sensors for breath testing: From nanomaterials to comprehensive disease detection. *Acc. Chem. Res.* **2014**, *47*, 66–76. [CrossRef] [PubMed]

24. Wu, L.; Qu, X. Cancer biomarker detection: Recent achievements and challenges. *Chem. Soc. Rev.* **2015**, *44*, 2963–2997. [CrossRef] [PubMed]
25. Aasi, A.; Aghaei, S.M.; Panchapakesan, B. A density functional theory study on the interaction of toluene with transition metal decorated carbon nanotubes: A promising platform for early detection of lung cancer from human breath. *Nanotechnology* **2020**, *31*, 415707. [CrossRef] [PubMed]
26. Aasi, A.; Mortazavi, B.; Panchapakesan, B. Two-dimensional PdPS and PdPSe nanosheets: Novel promising sensing platforms for harmful gas molecules. *Appl. Surf. Sci.* **2021**, *579*, 152115. [CrossRef]
27. Aasi, A.; Javahersaz, R.; Aghaei, S.M.; Panchapakesan, B. First-principles insight into two-dimensional palladium phosphide tellurium (PdPTe) monolayer as a promising scavenger for detecting SF6 decompositions. *J. Mater. Sci.* **2022**, *57*, 5497–5506. [CrossRef]
28. Kaur, S.; Kumar, A.; Srivastava, S.; Tankeshwar, K.; Pandey, R. Monolayer, bilayer, and heterostructures of green phosphorene for water splitting and photovoltaics. *J. Phys. Chem. C* **2018**, *122*, 26032–26038. [CrossRef]
29. Yang, G.; Ma, T.; Peng, X. Superior mechanical flexibility and strained-engineered direct-indirect band gap transition of green phosphorene. *Appl. Phys. Lett.* **2018**, *112*, 241904. [CrossRef]
30. Han, W.H.; Kim, S.; Lee, I.-H.; Chang, K.J. Prediction of green phosphorus with tunable direct band gap and high mobility. *J. Phys. Chem. Lett.* **2017**, *8*, 4627–4632. [CrossRef]
31. Mao, Z.; Dong, S.; Li, J.; Lin, X.; Jian, X.; Wu, P. Inorganic gas sensing of green phosphorene nanosheet: Insights from density functional theory. *J. Phys. Condens. Matter* **2020**, *32*, 355002. [CrossRef]
32. Kaewmaraya, T.; Ngamwongwan, L.; Moontragoon, P.; Jarernboon, W.; Singh, D.; Ahuja, R.; Karton, A.; Hussain, T. Novel green phosphorene as a superior chemical gas sensing material. *J. Hazard. Mater.* **2021**, *401*, 123340. [CrossRef] [PubMed]
33. Swetha, B.; Nagarajan, V.; Chandiramouli, R. Interaction Studies of Methanol and Ethanol Vapors on Green Phosphorene Sheets: A First-Principles Study. *ChemistrySelect* **2019**, *4*, 14237–14243. [CrossRef]
34. Aasi, A.; Javahersaz, R.; Aghaei, S.M.; Panchapakesan, B. Novel green phosphorene as a superior gas sensor for dissolved gas analysis in oil transformers: Using DFT method. *Mol. Simul.* **2022**, *48*, 541–550. [CrossRef]
35. Taylor, J.; Guo, H.; Wang, J. Ab initio modeling of quantum transport properties of molecular electronic devices. *Phys. Rev. B* **2001**, *63*, 245407. [CrossRef]
36. Brandbyge, M.; Mozos, J.-L.; Ordejón, P.; Taylor, J.; Stokbro, K. Density-functional method for nonequilibrium electron transport. *Phys. Rev. B* **2002**, *65*, 165401. [CrossRef]
37. Grimme, S. Semiempirical GGA-type density functional constructed with a long-range dispersion correction. *J. Comput. Chem.* **2006**, *27*, 1787–1799. [CrossRef]
38. Rad, A.S.; Abedini, E. Chemisorption of NO on Pt-decorated graphene as modified nanostructure media: A first principles study. *Appl. Surf. Sci.* **2016**, *360*, 1041–1046. [CrossRef]
39. Jia, X.; Zhang, H.; Zhang, Z.; An, L. Effect of doping and vacancy defects on the adsorption of CO on graphene. *Mater. Chem. Phys.* **2020**, *249*, 123114. [CrossRef]
40. Liu, H.; Lee, J.Y. Electric field effects on the adsorption of CO on a graphene nanodot and the healing mechanism of a vacancy in a graphene nanodot. *J. Phys. Chem. C* **2012**, *116*, 3034–3041. [CrossRef]
41. Bhuvaneswari, R.; Nagarajan, V.; Chandiramouli, R. Novel green phosphorene sheets to detect tear gas molecules-A DFT insight. *J. Mol. Graph. Model.* **2020**, *100*, 107706. [CrossRef]
42. Mao, Z.; Dong, S.; Li, J.; Lin, X.; Jian, X.; Wu, P. Applied biaxial strain induced tunable sensing performance of green phosphorene monolayer towards small molecules: A DFT study. *Appl. Surf. Sci.* **2021**, *536*, 147759. [CrossRef]
43. Mata, F.; Martin, M.C.; Sørensen, G.O. Microwave spectra of deuterated furans. Revised molecular structure of furan. *J. Mol. Struct.* **1978**, *48*, 157–163. [CrossRef]
44. Venkatesh, G.; Govindaraju, M.; Kamal, C.; Vennila, P.; Kaya, S. Structural, electronic and optical properties of 2, 5-dichloro-p-xylene: Experimental and theoretical calculations using DFT method. *RSC Adv.* **2017**, *7*, 1401–1412. [CrossRef]
45. Fan, G.; Wang, X.; Tu, X.; Xu, H.; Wang, Q.; Chu, X. Density functional theory study of Cu-doped BNNT as highly sensitive and selective gas sensor for carbon monoxide. *Nanotechnology* **2020**, *32*, 075502. [CrossRef]
46. Pitt, I.G.; Gilbert, R.G.; Ryan, K.R. Application of transition-state theory to gas-surface reactions: Barrierless adsorption on clean surfaces. *J. Phys. Chem.* **1994**, *98*, 13001–13010. [CrossRef]
47. Du, J.; Jiang, G. First-principle study on monolayer and bilayer SnP3 sheets as the potential sensors for NO2, NO, and NH3 detection. *Nanotechnology* **2020**, *31*, 325504. [CrossRef]